MOLECULAR AND CELLULAR BIOLOGY, Dec. 2010, p. 5686–5697 Vol. 30, No. 24
0270-7306/10/$12.00 doi:10.1128/MCB.00975-10

The Mammalian Sin3 Proteins Are Required for Muscle Development and Sarcomere Specification▽†

Chris van Oevelen,[1]‡ Christopher Bowman,[1]‡ Jessica Pellegrino,[1] Patrik Asp,[1] Jemmie Cheng,[1] Fabio Parisi,[1] Mariann Micsinai,[1] Yuval Kluger,[1] Alphonse Chu,[2] Alexandre Blais,[2] Gregory David,[1]* and Brian D. Dynlacht[1]*

Departments of Cell Biology, Pharmacology, and Pathology, NYU School of Medicine, 550 First Avenue, New York, New York 10016,[1] and Ottawa Institute of Systems Biology, 451 Smyth Road, Ottawa, Ontario K1H 8M5, Canada[2]

Received 19 August 2010/Returned for modification 21 September 2010/Accepted 6 October 2010

The highly related mammalian Sin3A and Sin3B proteins provide a versatile platform for chromatin-modifying activities. Sin3-containing complexes play a role in gene repression through deacetylation of nucleosomes. Here, we explore a role for Sin3 in myogenesis by examining the phenotypes resulting from acute somatic deletion of both isoforms *in vivo* and from primary myotubes *in vitro*. Myotubes ablated for Sin3A alone, but not Sin3B, displayed gross defects in sarcomere structure that were considerably enhanced upon simultaneous ablation of both isoforms. Massively parallel sequencing of Sin3A- and Sin3B-bound genomic loci revealed a subset of target genes directly involved in sarcomere function that are positively regulated by Sin3A and Sin3B proteins. Both proteins were coordinately recruited to a substantial number of genes. Interestingly, depletion of Sin3B led to compensatory increases in Sin3A recruitment at certain target loci, but Sin3B was never found to compensate for Sin3A loss. Thus, our analyses describe a novel transcriptional role for Sin3A and Sin3B proteins associated with maintenance of differentiated muscle cells.

In mammalian cells, the Sin3 core complex, which consists of at least eight subunits, including Sin3A, Sin3B, and the histone deacetylases (HDAC1 and HDAC2), transiently associates with other regulatory proteins, including pRB and chromatin regulatory enzymes, to control gene expression (36). Sin3-HDAC complexes are recruited by sequence-specific transcription factors to promoter regions, resulting in localized deacetylation of histones and transcriptional silencing (1, 2, 15, 17, 20, 30, 32, 39). However, growing evidence suggests that Sin3-HDAC complexes may also function on active genes. Specifically, Sin3-HDAC complexes recently identified in budding and fission yeast were shown to deacetylate nucleosomes within the coding regions of transcribed genes, preventing spurious sense and antisense transcription (8, 18, 27). In mammalian cells, expression analyses demonstrated that acute somatic deletion of *Sin3A* resulted in the downregulation of a significant number of genes (12). Recently, we used ChIP-on-chip experiments (chromatin immunoprecipitation [ChIP] combined with microarray hybridization) to map Sin3A and Sin3B binding sites in differentiated C2C12 myotubes (Mt) and identified two classes of target genes bound by Sin3A and Sin3B in myotubes. The first class of genes was bound by both E2F4 and Sin3A/B and was repressed during differentiation, and this cluster was enriched for cell cycle, DNA repair, and DNA damage checkpoint genes. In contrast, the second group of genes was bound by Sin3A/B but not E2F4. This cluster was enriched for genes involved in metabolic pathways, differentiation, and development, and depletion of Sin3 isoforms did not result in transcriptional derepression.

Genetic inactivation of Sin3A or Sin3B in mice revealed essential and nonredundant functions for Sin3 proteins at different stages of mouse development. Sin3A-null embryos died early during embryogenesis, preventing the elucidation of Sin3A function during cellular differentiation (10, 12). In contrast, Sin3B is dispensable during early development but essential at later stages, since Sin3B-null mice exhibited striking defects in blood cell maturation and skeletal development, processes linked to cell cycle exit (13). Sin3A and Sin3B homologs have also been implicated in diverse developmental pathways in *Drosophila* species and *Caenorhabditis elegans* (11, 25, 35).

To further explore the developmental role of mammalian Sin3-containing complexes in a well-characterized system, namely, muscle differentiation, we have generated mice and cells that are somatically inactivated for Sin3A, Sin3B, or both. The phenotypes resulting from this inactivation definitively demonstrate distinct roles for Sin3A and Sin3B isoforms in maintaining myofibril structure and function in the postdifferentiated state. Furthermore, unbiased identification of targets bound by Sin3A and Sin3B during muscle differentiation revealed a cohort of genes involved in assembly of sarcomeres, the basic unit of muscle contraction. Expression of these target genes was significantly reduced upon ablation of Sin3 isoforms, providing new insights into the contribution of Sin3 proteins to transcriptional activation of genes required for myogenesis and muscle integrity.

* Corresponding author. Mailing address: Department of Pathology, New York University School of Medicine, 550 First Avenue, New York, NY 10016. Phone for Gregory David: (212) 263-2926. Fax: (212) 263-7133. E-mail: gregory.david@med.nyu.edu. Phone for Brian D. Dynlacht: (212) 263-6162. Fax: (212) 263-6157. E-mail: brian.dynlacht@med.nyu.edu.

† Supplemental material for this article may be found at http://mcb.asm.org/.

‡ C. van Oevelen and C. Bowman contributed equally to this study.

▽ Published ahead of print on 18 October 2010.

MATERIALS AND METHODS

Mice and cell culture. Mice harboring floxed alleles of Sin3A and Sin3B and *Myf5-Cre* and *MCK-Cre* transgenes were described previously (6, 12, 13, 38). C2C12 cells (obtained from the ATCC) were cultured as described previously (4). Primary myoblasts were isolated according to previous methods (29), except that cells were grown on plates coated with a 1:10 solution of BD Matrigel (BD254248). Cells were grown to near confluence before being switched to differentiation-inducing medium (Dulbecco's modified Eagle's medium [DMEM]-5% horse serum).

Viral infections, RNA interference (RNAi), RT-PCR, and IF. Primary myoblasts were grown to near confluence, at which time the medium was changed to DMEM supplemented with 5% horse serum to induce differentiation. After 48 h in differentiation medium, primary myotubes were infected with control adenovirus or virus expressing Cre recombinase (Gene Transfer Vector Core, University of Iowa) at a multiplicity of infection (MOI) of 100 for 24 h. After 24 h, the primary myotubes were grown for an additional 48 h before being prepared for reverse transcription-PCR (RT-PCR) and immunofluorescence (IF). C2C12 cells were grown and transfected as previously described (39). RT-PCR was performed using 250 ng of total RNA per reverse transcriptase reaction (Invitrogen). cDNA was diluted and quantified twice by real-time PCR using the SYBR green method. For immunofluorescence, the cells were fixed in 10% neutral buffered formalin solution. Anti-alpha-actinin α2 antibody (1:1,500; Sigma A7811) and a Cy3 anti-mouse secondary antibody (1:500) were used.

EM. Five-day-old mice were perfused with a 0.1 M phosphate buffer (pH 7.3) containing 2.5% electron microscopy (EM)-grade glutaraldehyde (GA) and 4% paraformaldehyde (PFA). Gastrocnemius was dissected and fixed overnight in a 0.1 M phosphate buffer (pH 7.3) solution containing 1% EM-grade GA. Primary myotubes were fixed with a 0.1 M phosphate buffer (pH 7.3) containing 2.5% EM-grade GA and 4% PFA. Sixty-nanometer sections were collected and stained with 3% uranyl acetate in 50% methanol and lead citrate. Images were captured on a Philips CM12 transmission electron microscope (TEM) at 120 kV with a 4K- by 2.67K-pixel Gatan digital camera.

Immunohistochemistry. To isolate gastrocnemius muscle from euthanized 5-day-old mice, hind limbs were dissected and stored in 4% PFA in phosphate-buffered saline (PBS) at 4°C for 24 h and then transferred to 10% sucrose for 24 h at 4°C. Limbs were frozen on dry ice and then embedded in Tissue-Tek OCT compound in aluminum foil molds and set in dry ice. Samples were cut in 8-μm cryosections using a cryostat (Microm 560; Thermo Scientific), mounted on gelatin-coated glass slides, and incubated at room temperature overnight. Slides were stored at −80°C until staining. For immunofluorescence, slides were dried, permeabilized with 0.2% TritonX-100 in PBS, and rinsed in PBS-Tween 20. Sections were blocked in 5% sheep serum (sc-2488; Santa Cruz Biotechnology) in PBS-Tween 20 for 30 min and rinsed in PBS-Tween 20. Sections were incubated with primary antibodies against α-actinin (Sigma A7811, clone EA-53) overnight in wet chambers at 4°C. Slides were washed with PBS-Tween 20. Sections were incubated with secondary antibody (Alexa Fluor 488 A1101; Invitrogen) and washed with PBS-Tween 20. Sections were incubated with TO-PRO-3 iodide (T3605; Invitrogen), rinsed in PBS, and mounted with Vectashield with DAPI (4′,6-diamindino-2-phenylindole) (H-1200; Vector Laboratories, Inc.). Images were acquired using a confocal microscope (Axiovert 200M, LSM 510 laser scanning microscope; Carl Zeiss, Inc.) with a 40×/0.75-numerical-aperture Plan/Neofluar objective using LSM 510 software (Carl Zeiss, Inc.). Images were processed using Photoshop CS3 (Adobe).

ChIP sequencing. Cells were cross-linked, harvested, and lysed as described previously (37). For conventional ChIP, nuclei were collected by centrifugation, resuspended in sonication buffer (1 mM EDTA, 0.5 mM EGTA, 10 mM Tris [pH 8], 0.5% *N*-lauroyl-sarcosine, and protease inhibitors), and sonicated on ice to an average length of 350 bp. Antibodies against Sin3A (sc-767), Sin3B (sc-768), and E2F4 (sc-1082) were obtained from Santa Cruz. Antibody against HDAC1 (06-720) was obtained from Millipore. To isolate mononucleosomal chromatin fragments, nuclei were resuspended in MNase buffer (10 mM Tris at pH 7.4, 60 mM KCl, 15 mM NaCl, 2 mM $CaCl_2$), briefly washed, and treated with ~150 U MNase (Worthington) at room temperature for 30 min. The reaction was quenched with 10 mM EDTA and sonicated. Cross-links were reversed, and DNA was extracted according to the ChIP protocol. Antibodies against histone H3K4-3 M (ab8580) and anti-H3Ac (K9Ac-K14Ac and 06-599) were obtained from Abcam and Millipore. DNA libraries were prepared for immunoprecipitation (IP) and corresponding input samples per Illumina's instructions. Libraries were sequenced using a Solexa 2G genome analyzer in accordance with the manufacturer's protocols. Images were processed using the Illumina pipeline to generate raw sequence files, which were subsequently aligned to the mouse genome (mm9) without mismatches. Aligned sequences were further filtered to remove identical sequence tags and sequence tags that do not align uniquely to the mouse genome. To detect regions of enrichment characterized by increased sequence tag density relative to the measured background, we employed model-based analysis of ChIP combined with massively parallel sequencing (MACS) using a minimum cutoff of 8 tags per enriched region and a P value of $<1 \times 10^{-7}$ (41).

Gene expression profiling. Growing C2C12 cells were induced to differentiate, and the resulting cells were processed as described previously (4). Microarray data can be downloaded from the Gene Expression Omnibus under accession number GSE19968. RNA was extracted and purified with an Absolutely RNA miniprep kit (Stratagene) in accordance with the manufacturer's recommendations. The cells were lysed in the presence of 0.7% of β-mercaptoethanol and treated with DNase I. For both the time course and the RNAi samples, experiments were performed on at least three independent biological replicates. Gene expression profiling was done using the one-color microarray gene expression platform from Agilent Technologies. The 4x44k whole-mouse genome oligonucleotide microarray was used. Labeled cDNA was made using a Quick Amp one-color labeling kit (Agilent). In accordance with the manufacturer's protocol, 300 ng of RNA was labeled and used for each microarray. The slides were hybridized at 65°C for at least 17 h, washed, and scanned per the manufacturer's instructions. After the slides were scanned, the intensities of the spots were extracted using Feature Extraction version 10.1.1. Raw median probe intensities were normalized using GeneSpring GX version 10.0 (Agilent Technologies), first by scaling probe signals within each microarray to the 75th percentile of the respective sample, then by eliminating probes with no or marginal signal in all samples, and finally by averaging the normalized signal among replicate samples.

Immunoprecipitations. Nuclear extracts were prepared as previously described (9), with the following modifications. The hypotonic homogenization buffer was adjusted to 7 mM KCl, and the nuclear extraction buffer was adjusted to 0.42 M KCl. One milligram of nuclear extract was immunoprecipitated with 1 μg of antibodies cross-linked to a mixture of protein A/G-Sepharose and washed with nuclear extraction buffer containing 0.15 M KCl. Precipitated material was separated on an 8% SDS-PAGE gel together with 50 μg of nuclear extract as an input and blotted to polyvinylidene difluoride (PVDF). Antibodies against Sin3A (sc-767) and Sin3B (sc-768) were obtained from Santa Cruz. Antibodies against pRb (monoclonal antibodies 21C9 and 554136) were obtained from R. Weinberg and Pharmingen and were used for immunofluorescence and Western blotting, respectively.

RESULTS AND DISCUSSION

Acute somatic deletion of Sin3A and Sin3B *in vivo* reveals an essential role in muscle biology. Our previous studies demonstrated that Sin3A and Sin3B bind to overlapping and distinct sets of target genes in myotubes derived from C2C12 myoblasts *in vitro* (39). To unambiguously delineate the specific contributions of Sin3A and Sin3B to muscle differentiation and physiology *in vivo*, we crossed mice harboring Sin3A and Sin3B conditional alleles to transgenic mice expressing the Cre recombinase in the myoblast compartment (*Myf5-Cre*) or in differentiated skeletal muscle cells (*MCK-Cre*). Expression of the Cre recombinase thus results in efficient and rapid inactivation of the conditional Sin3A or Sin3B allele at different stages of embryonic development (6, 12, 13, 38). We found that somatic inactivation of Sin3A or Sin3B in myoblasts led to strikingly different phenotypes. *Myf5-Cre*::*Sin3A*$^{f/-}$ mice died perinatally, and no viable pups were present 24 h after birth. In contrast, *Myf5-Cre*::*Sin3B*$^{f/-}$ mice were observed with expected Mendelian proportions and survived for up to 2 years (the length of the experiment) with no obvious developmental defects (data not shown).

Interestingly, viable Sin3A$^{f/-}$ or Sin3B$^{f/-}$ pups bearing the *MCK-Cre* transgene were identified with expected Mendelian ratios up to 5 days after birth. However, the vast majority of mice deleted for Sin3A in skeletal muscle (Sin3A$^{f/-}$; Sin3B$^{f/+}$; MCK-Cre^{+}, here referred to as Sin3A$^{-/-}$; Sin3B$^{+/-}$) and mice deleted for both Sin3A and Sin3B (Sin3A$^{f/-}$; Sin3B$^{f/-}$; MCK-

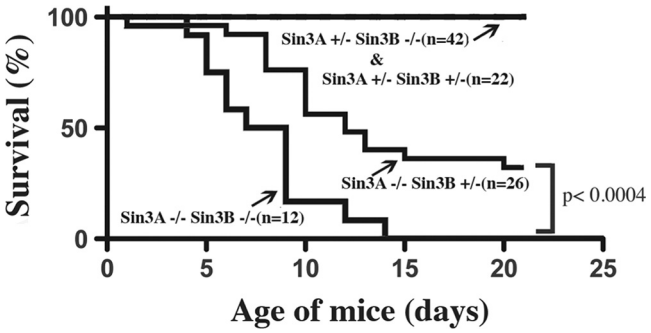

FIG. 1. Survival rates of mice conditionally deleted for *Sin3* genes. Mice carrying floxed alleles of Sin3A or Sin3B were crossed with *MCK-Cre* transgenic mice to yield $Sin3A^{+/-}$; $Sin3B^{+/-}$, $Sin3A^{+/-}$; $Sin3B^{-/-}$, $Sin3A^{-/-}$; $Sin3B^{+/-}$, and $Sin3A^{-/-}$; $Sin3B^{-/-}$ mice. Mice showed isoform-specific differences in viability. Ablation of both Sin3A and Sin3B decreased viability significantly (log rank [Mantel-Cox] test).

Cre^+, here referred to as $Sin3A^{-/-}$; $Sin3B^{-/-}$) died within the first 2 weeks of life. The median survival periods for Sin3 mutant mice were 12 and 8 days for $Sin3A^{-/-}$; $Sin3B^{+/-}$ and $Sin3A^{-/-}$; $Sin3B^{-/-}$ mice, respectively (Fig. 1). In contrast, mice deleted for Sin3B in skeletal muscle ($Sin3A^{f/+}$; $Sin3B^{f/-}$; MCK-Cre^+, here referred to as $Sin3A^{+/-}$; $Sin3B^{-/-}$) were phenotypically indistinguishable from control mice ($Sin3A^{f/+}$; $Sin3B^{f/+}$; MCK-Cre^+, here referred to as $Sin3A^{+/-}$; $Sin3B^{+/-}$) up to 12 months of age (Fig. 1). Thus, mice with combined deletions of Sin3A and Sin3B, driven by the MCK-Cre transgene, exhibited significant decreases in duration of survival compared to mice with single deletions of Sin3A (or Sin3B) (Fig. 1) ($P < 0.05$). Transgenic *MCK-Cre* mice ablated for *Sin3A* or both *Sin3* isoforms did not exhibit overt respiratory defects and did not appear cyanotic, nor did we observe noticeable differences in nursing behavior compared to that of littermates. The cause of death of Sin3A- and Sin3A/B-deleted pups remains unknown and may reflect leaky expression of the Cre transgene in tissues other than skeletal muscle. Nevertheless, these observations indicate that combined deletion of Sin3A and Sin3B, mediated by the MCK-Cre transgene, leads to a significant decrease in survival compared to single deletions of Sin3A (or Sin3B) (Fig. 1) ($P < 0.05$). This observation represents, to our knowledge, the first demonstration that Sin3A and Sin3B share redundant functions in a defined physiological setting.

Depletion of Sin3 from skeletal muscle results in sarcomere disruption. To more precisely address the specific contributions of Sin3A and Sin3B to muscle differentiation and physiology *in vivo*, skeletal muscle tissue of *MCK-Cre* transgenic mice was dissected from littermates of all genotypes at day 5, before the pups exhibited any abnormalities. Upon histological examination of hematoxylin and eosin (H&E)-stained sections, we observed gross structural defects in tissue lacking Sin3A or both Sin3 isoforms (data not shown).

We analyzed sarcomere organization more closely using immunofluorescence (IF) and electron microscopy (EM) (see Materials and Methods). For IF analysis, we used an antibody against skeletal muscle actinin α2, a marker for Z discs within the sarcomere. Muscle tissue from hind limbs (gastrocnemius) of control mice ($Sin3A^{+/-}$; $Sin3B^{+/-}$) or mice deleted for Sin3B ($Sin3A^{+/-}$; $Sin3B^{-/-}$) showed a regular, striated pattern of α-actinin-stained Z discs, characteristic of normal muscle fibers (Fig. 2A). In contrast, staining of muscle tissue derived from mice deleted for Sin3A ($Sin3A^{-/-}$; $Sin3B^{+/-}$) or for both proteins ($Sin3A^{-/-}$; $Sin3B^{-/-}$) showed an irregular α-actinin-stained Z-disc pattern within large sections of the myofibril, most likely reflecting disorganized sarcomeres (Fig. 2A). Importantly, as the *MCK-Cre* transgene is active in postmitotic, differentiated muscle cells but not during myogenesis, these results point to an essential role for Sin3A in maintaining sarcomere organization in differentiated cells.

Next, we used EM to document the ultrastructural features and, more specifically, the integrity of sarcomeres in myotubes deleted for Sin3A, Sin3B, or both proteins. In agreement with our IF analyses, muscle tissue derived from the gastrocnemius of control mice or mice deleted for Sin3B showed a regular arrangement of sarcomeric units, with distinct Z discs, A and I bands, and M lines (Fig. 2B). In contrast, we observed a dramatic overall disruption of sarcomeric architecture within muscle tissue derived from mice deleted for both Sin3A and Sin3B, resulting in irregular myofibrillar arrays. Interestingly, this phenotype was less penetrant in Sin3A-deleted muscle than in muscle ablated for both Sin3A and Sin3B, as only one pup out of two exhibited defects in sarcomere organization at day 5. In the affected Sin3A-deleted animals or in the animals deleted for Sin3A and Sin3B, sarcomeres were characterized by disrupted Z discs and dissociation of I bands (Fig. 2B, third and fourth rows). Furthermore, many of the filaments within Sin3A- and Sin3B-deleted fibers end abruptly without proper termination in the Z disc. Finally, we observed widespread dissociation of fibers and large interstitial spaces in the sarcoplasm surrounding the myofibrils (Fig. 2B, third and fourth rows). Thus, our results point to a previously unknown role for Sin3 isoforms in maintaining the subcellular structure and integrity of myofibers. Interestingly, in contrast with conditional deletion of Sin3A or both Sin3 isoforms, somatic deletion of *Rb* in mice with the same *MCK-Cre* transgene used in our study did not result in any overt phenotype (16), suggesting that Sin3 complexes required for myofibril organization are functionally separable from those involving pRB.

Ablation of Sin3 in primary myotubes leads to sarcomeric defects. In order to assess whether the sarcomeric phenotypes elicited upon inactivation of Sin3A and Sin3B proteins in muscle tissue result from cell-autonomous defects, we isolated primary myoblasts from mice harboring combinations of conditional *Sin3A* or *Sin3B* alleles ($Sin3A^{f/-}$; $Sin3B^{f/+}$, $Sin3A^{f/+}$; $Sin3B^{f/-}$, and $Sin3A^{f/-}$; $Sin3B^{f/-}$). Primary myoblasts were cultured *in vitro*, and differentiation into myotubes was induced at confluence. Differentiated myotubes were then infected with an adenovirus expressing Cre (*Ad-Cre*) or a control adenovirus lacking Cre (vector) 48 h after induction of differentiation. Excision of floxed *Sin3A* and *Sin3B* exons was assessed by measuring mRNA levels using quantitative RT-PCR (qRT-PCR) at 48 h postinfection. We observed strong and specific decreases in Sin3A and Sin3B mRNA levels after infection with Ad-Cre but not with the control virus (Fig. 3A). We did not observe compensatory upregulation of the remaining isoform after ablation of the other (Fig. 3A).

Ad-Cre- or control-infected primary myotubes were stained

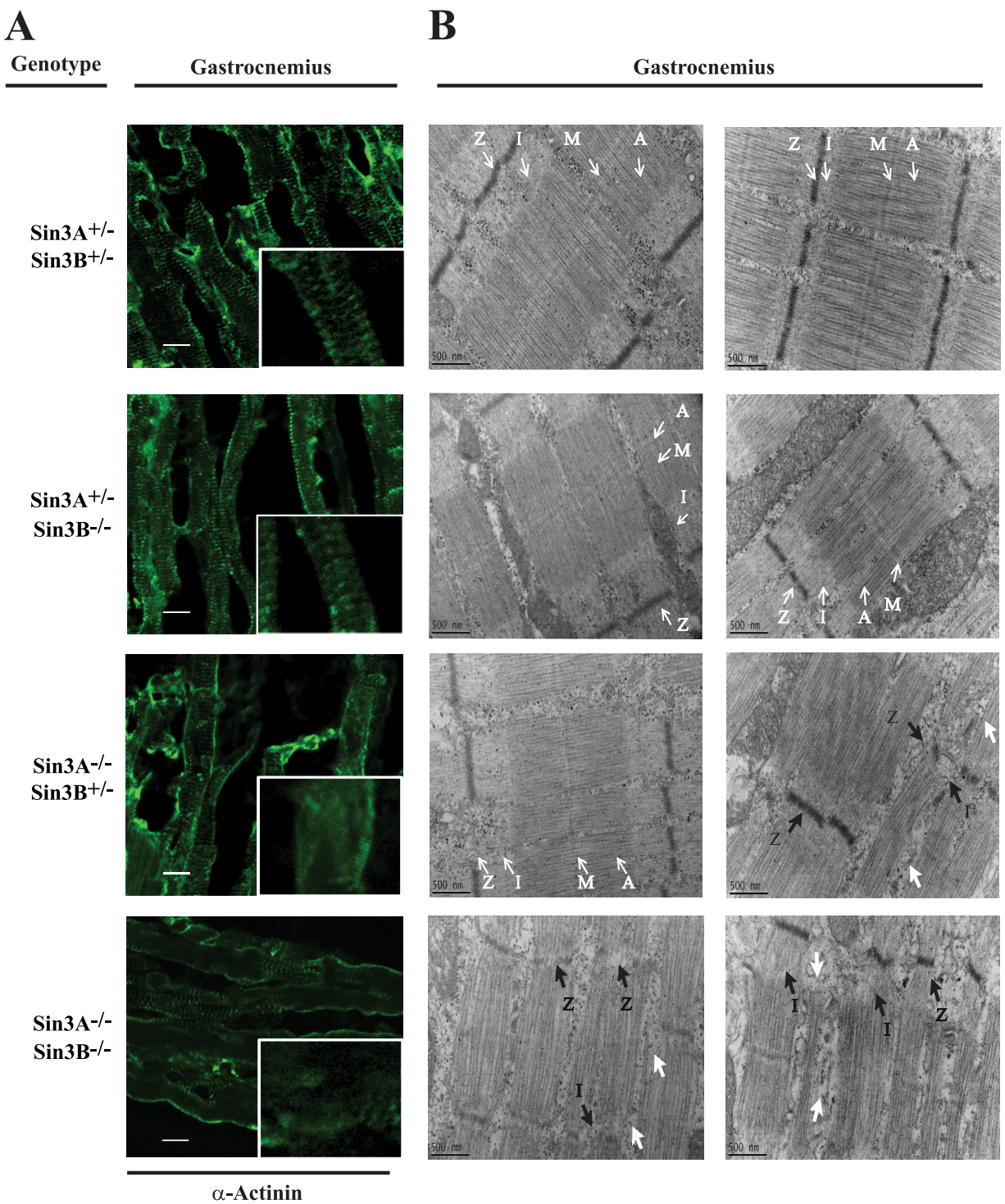

FIG. 2. Conditional ablation of Sin3 in mouse skeletal muscle provokes severe myofibril defects. Skeletal muscles (gastrocnemius) of floxed *MCK-Cre*::*Sin3* mice were dissected at postnatal day 5 and processed for either immunohistochemistry or electron microscopy (EM). (A) Immunofluorescence detection of α-actinin α2 in longitudinal sections of skeletal muscle cells of *Sin3A*$^{+/-}$; *Sin3B*$^{+/-}$ (control), *Sin3A*$^{+/-}$; *Sin3B*$^{-/-}$, *Sin3A*$^{-/-}$; *Sin3B*$^{+/-}$, and *Sin3A*$^{-/-}$; *Sin3B*$^{-/-}$ mice. White squares indicate selected regions shown at higher magnification. Bar, 10 μM. (B) EM analysis of longitudinal sections of skeletal muscle tissue from two different mice from each genotype (first and second columns). The genotypes are identical to those in panel A. Ablation of Sin3A or both Sin3A and Sin3B resulted in severe structural aberrations. White arrows with unfilled arrowheads indicate normal sarcomeric structures. Black and white arrows with solid arrowheads indicate structural abnormalities: black solid arrows indicate disrupted Z discs and I bands, and white solid arrows point to dissociated fibers and large interstitial spaces in between myofibrils. A, A band; I, I band; M, M line; Z, Z disc. Bar, 500 nm.

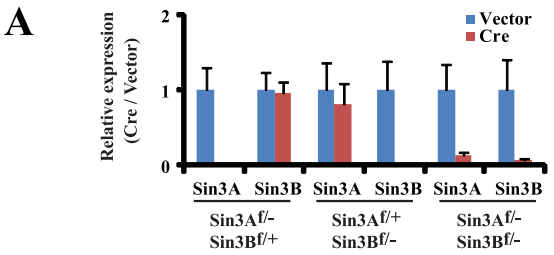
A
Relative expression (Cre / Vector)
2
1
0
Vector
Cre
Sin3A Sin3B Sin3A Sin3B Sin3A Sin3B
Sin3Af/- Sin3Bf/+
Sin3Af/+ Sin3Bf/-
Sin3Af/- Sin3Bf/-

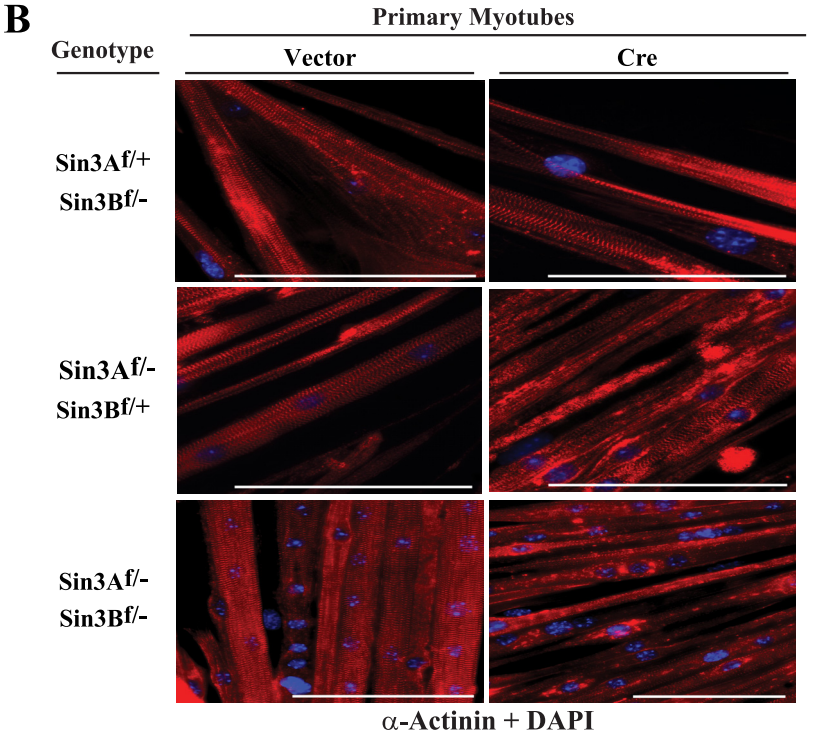
B
Primary Myotubes
Genotype
Vector
Cre
Sin3Af/+ Sin3Bf/-
Sin3Af/- Sin3Bf/+
Sin3Af/- Sin3Bf/-
α-Actinin + DAPI

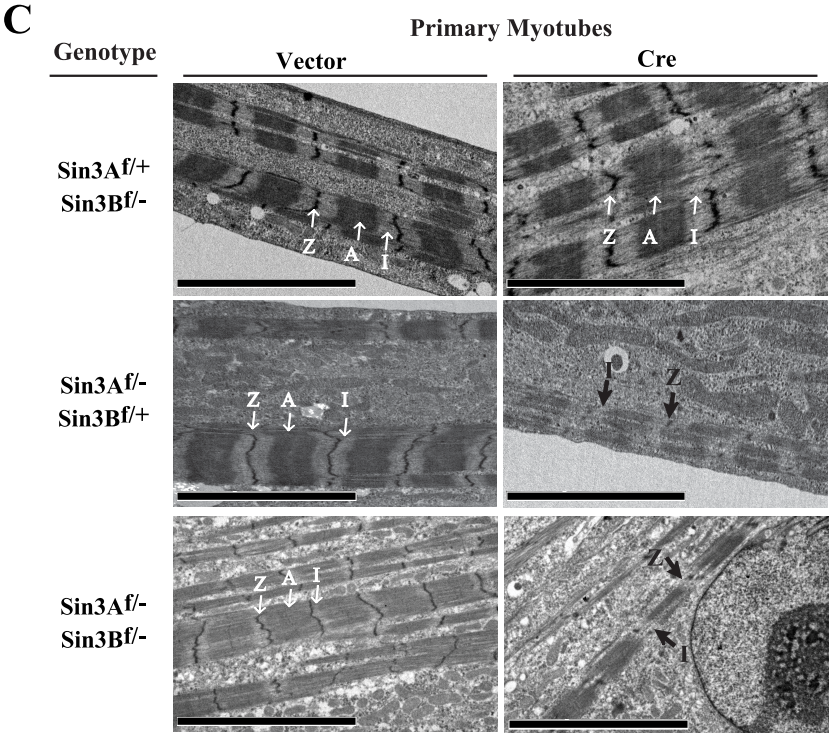
C
Primary Myotubes
Genotype
Vector
Cre
Sin3Af/+ Sin3Bf/-
Sin3Af/- Sin3Bf/+
Sin3Af/- Sin3Bf/-
Z
A
I

for α-actinin and analyzed by fluorescence microscopy. All primary myotubes infected with control adenovirus showed regular arrays of α-actinin-stained Z discs, and similar results were obtained for Sin3B-depleted primary myotubes (Fig. 3B). In striking contrast, a large fraction of primary myotubes ablated for Sin3A or for both Sin3A and Sin3B were characterized by a loss of α-actinin-stained Z discs, and when they were present, Z discs appeared irregular (Fig. 3B). Next, we used EM to further analyze sarcomere structure upon deletion of Sin3A, Sin3B, or both proteins. Primary myotubes infected with the control adenovirus or primary myotubes deleted for Sin3B displayed regular sarcomeres with characteristic Z-disc, A-band, and I-band patterns (Fig. 3C). In contrast, primary myotubes ablated for Sin3A or for both Sin3 isoforms were characterized by thinner myofibrils and disruption or disappearance of Z discs. Remarkably, in a subset of these sarcomeres, A and I bands were not distinguishable (Fig. 3C).

In summary, acute inactivation of Sin3A and Sin3B in differentiated primary cells recapitulates the phenotypes observed in muscle tissue, indicating an essential and specific cell-autonomous role for Sin3 proteins in assembling sarcomeres and/or maintaining sarcomere integrity.

Recruitment of Sin3A and Sin3B during myogenesis. We previously identified Sin3A and Sin3B target genes in differentiated myotubes using ChIP-on-chip experiments with promoter DNA and tiling arrays (39). However, these arrays were limited to a portion of the mouse genome and did not cover intergenic and downstream coding regions. In order to identify the full range of Sin3A and Sin3B binding events during myogenesis, we combined ChIP with massively parallel sequencing (ChIP-seq) in fully differentiated C2C12 myotubes (Mt). On average, 4.4 million sequenced tags were uniquely aligned to the mouse genome after immunoprecipitation of Sin3A or Sin3B. Importantly, the increased coverage and resolution afforded by ChIP-seq allowed us to substantially extend our findings with regard to Sin3 isoform-specific recruitment (see below). To identify regions enriched for Sin3 binding, we used an algorithm, model-based analysis of ChIP-seq (MACS), with a minimal tag cutoff of 8 tags and a P value of $<1 \times 10^{-7}$ (41). We identified 1,491 and 4,993 targets for Sin3A and Sin3B, respectively (see Table S1 in the supplemental material). This represents a vast increase in the number of identified Sin3 target genes. A comparison of Sin3A and Sin3B binding sites indicated that 86% of Sin3A target sites were also bound by Sin3B in myotubes, although a large number (74%) of Sin3B targets did not overlap with Sin3A targets (Fig. 4A). Thus, our data strongly suggest the existence of distinct Sin3A and Sin3B complexes, whose recruitment to discrete targets is likely to depend on Sin3A- or Sin3B-specific interacting partners.

Our ChIP-on-chip experiments revealed that Sin3A and Sin3B binding occurs primarily downstream of the transcription start site (TSS) in differentiated myotubes (39). We therefore analyzed the distribution of Sin3A and Sin3B binding events in differentiated myotubes on the basis of our ChIP-seq data, which interrogated intergenic and downstream coding regions that had not been analyzed previously. Binding sites were annotated to the nearest transcription start site, and distances between median peak positions and the TSSs of all RefSeq genes were calculated. In agreement with our previous findings, we found that Sin3A and Sin3B primarily occupied regions close to the TSS (bp −3000 to +3000), with a strong positional bias downstream of the TSS (Fig. 4B).

We performed genome-wide expression profiling with myotubes and growing myoblasts and compared binding by Sin3A, Sin3B, or both with dynamic changes in gene expression during myogenesis. We found that a cluster of genes bound by both Sin3A and Sin3B in differentiated myotubes was significantly more repressed than a control set by testing the hypergeometric distribution ($P = 2 \times 10^{-21}$) (Fig. 4C, left panel), and a subset of these repressed genes play a role in cell cycle progression as previously reported (39). In contrast with genes bound by Sin3A and Sin3B, a cluster of targets bound by Sin3B displayed an enhanced and significant preference toward gene activation ($P = 3 \times 10^{-36}$) (Fig. 4C, right panel). This analysis further underscores the existence of distinct functions for Sin3 proteins in differentiated cells.

Sin3A and Sin3B bind to a cluster of sarcomere genes. To assess whether genes bound by Sin3 proteins function in different physiological pathways, we clustered our ChIP-seq targets using DAVID, a gene ontology (GO) program (14), and assessed the significance of enrichment for GO terms (Fig. 5A). Genes bound by Sin3A and Sin3B proteins were most significantly enriched in categories related to cell cycle regulation ($P = 4 \times 10^{-32}$), chromosome/chromatin ($P = 6 \times 10^{-21}$), RNA processing ($P = 4 \times 10^{-18}$), and DNA replication/repair ($P = 4 \times 10^{-13}$). Genes bound by Sin3A did not show any enrichment for a specific GO category, and genes bound by Sin3B were most enriched in categories related to RNA processing ($P = 5 \times 10^{-32}$), mitochondria/ER/redox ($P = 3 \times 10^{-30}$), protein catabolism ($P = 1 \times 10^{-29}$), and protein transport ($P = 1 \times 10^{-28}$). Interestingly, cell cycle and mitochondrial pathways targeted by Sin3 appear to be conserved through evolution on the basis of depletion and knockout experiments with *Saccharomyces cerevisiae*, *Drosophila*, and

FIG. 3. Primary myotubes ablated for Sin3 display severe defects in sarcoma structures. Primary myoblasts were isolated from *MCK-Cre*-negative *Sin3A*$^{f/-}$; *Sin3B*$^{f/+}$, *Sin3A*$^{f/+}$; *Sin3B*$^{f/-}$, and *Sin3A*$^{f/-}$; *Sin3B*$^{f/-}$ mice. Primary myoblasts were induced to differentiate, and primary myotubes were infected 48 h after induction of differentiation with adenovirus without (Vector [control]) or with (Cre) Cre recombinase and processed for RT-PCR, immunofluorescence, and EM. (A) Gene expression analysis using quantitative real-time RT-PCR of Sin3A and Sin3B genes after ablation of Sin3A or Sin3B. The expression levels of vector- and Cre-infected cells were normalized to the level for Rbp2, which is expressed at high levels and is not bound by Sin3 in differentiated myotubes. Normalized Cre values were compared with normalized control values. Averages of results from three independent experiments are shown. Error bars represent standard deviations. (B) Immunofluorescence detection of α-actinin α2 and DAPI staining in primary myotubes ablated for Sin3A, Sin3B, or both Sin3A and Sin3B. Bar, 100 μm. (C) EM analyses of longitudinal sections of primary myotubes. Genotypes are as described for panel A. Ablation of Sin3A or both Sin3A and Sin3B resulted in significant structural alterations. White arrows indicate normal sarcomeric structures. Black arrows indicate structural abnormalities. A, A band; I, I band; Z, Z disc. Bar, 5 μm.

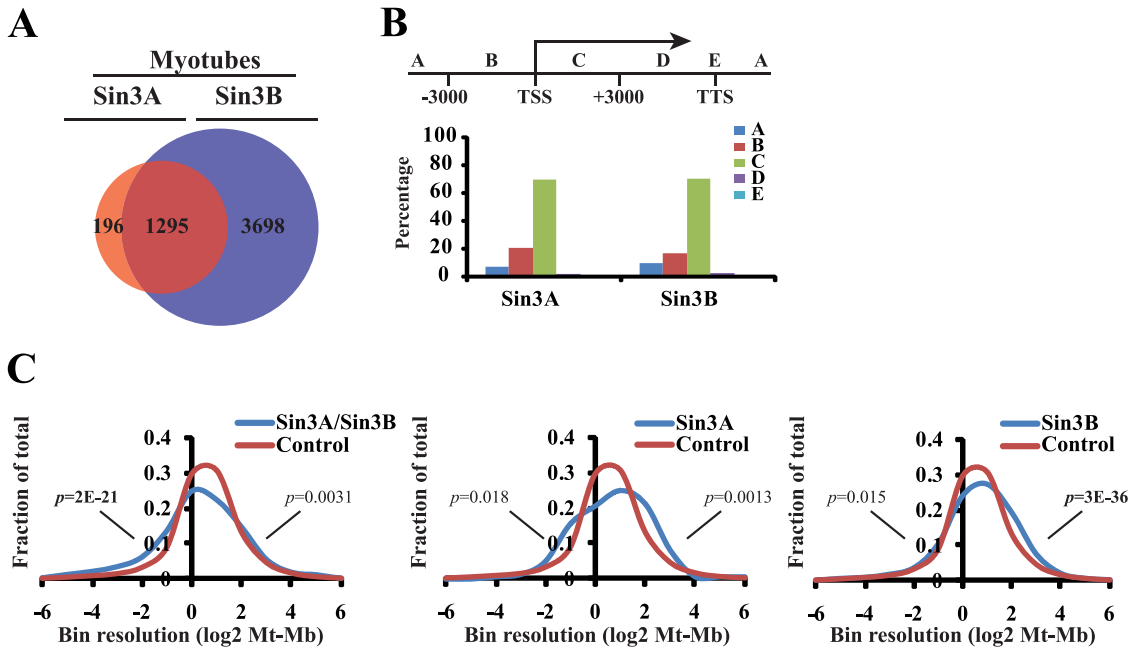

FIG. 4. Identification and characterization of Sin3 targets during myogenesis. (A) Venn diagrams showing overlap between Sin3A and Sin3B binding events in differentiated myotubes identified by ChIP-seq. Overlap between Sin3 binding sites was defined within a 250-bp interval. The results of two independent experiments were merged for a final analysis. Binding events were identified using MACS with a cutoff *P* value of $<1 \times 10^{-7}$ and a minimal tag cutoff of 8. (B) Genomic distribution of Sin3A and Sin3B binding events during myogenesis. (Upper panel) Definition of regions used to calculate genomic distribution of Sin3A and Sin3B binding events. Region A is without an upstream limit. (Lower panel) The distance of a binding event relative to the transcription start site (TSS) or transcription termination site (TTS) (group E only) was calculated using the median position of a binding event. The total number of peaks per region was expressed as a percentage of the total number of binding events. (C) Distribution of relative expression profiles during differentiation for genes bound by a combination of Sin3A or Sin3B in myotubes deduced from the ChIP-seq data. The numbers of genes bound per group were as follows: for Sin3A/Sin3B, 1,148; for Sin3A, 159; and for Sin3B, 2,994. The background group (Control) consisted of all genes defined in Refseq (version mm9). The hypergeometric distribution test was used to calculate statistical significance. *p*, *P* value; Mb, myoblasts; Mt, differentiated myotubes.

mammalian cells (12, 19, 28, 31). Using this approach, we also identified a cluster of Sin3 target genes specifically involved in muscle development, potentially relevant for our observed phenotypes in muscle tissue (Fig. 2) and primary myotubes (Fig. 3). We examined this group of Sin3 target genes more extensively, using gene ontology annotation as a reference (http://www.ebi.ac.uk/GOA/) (Fig. 5B). Strikingly, we identified 98 genes involved in muscle physiology, 40 of which were bound by both Sin3A and Sin3B (see Table S1 in the supplemental material; also Fig. 5B). Within this cluster of 98 genes, we had previously identified 22 genes by ChIP-on-chip experiments, including *Ttn*, *Tnnc1*, *Cfl2*, *Itga7*, *Snta1*, and *Nes* (39). Using quantitative ChIP (qChIP) analysis, we verified Sin3 binding in differentiated C2C12 cells and primary myotubes and confirmed binding of Sin3A and Sin3B to these genes (Fig. 5C and D).

Notably, Sin3 target genes identified in myotubes encode different components of the sarcomere, including the titin (*ttn*), troponin C1 (*tnnc1*), and desmin (*des*) genes, among others (Fig. 5B), and several of these genes have been implicated in a wide variety of skeletal myopathies (7, 21, 26). In addition, we identified the integrin alpha 7 and integrin beta 1 genes (*itgα7* and *itgβ1*, respectively) as Sin3A/B target genes in myotubes. Itgα7 and Itgβ1 heterodimers are cell surface receptors and interact with the extracellular matrix (ECM). Muscle integrins Itgα7 and Itgβ1 are enriched at myotendinous and neuromuscular junctions and are important for the formation and integrity of these complexes. Furthermore, the integrin α7β1 heterodimer and downstream effectors talin1 and vinculin provide lateral linkage of the cytoskeleton via costameric complexes to the sarcolemma, which is important for muscle integrity (7, 33). We also identified the dystroglycan 1 (*dag1*) and syntrophin (*snta1* and *sntb1*) genes, which are part of the dystrophin glycoprotein complex (DGC), as Sin3A/B target genes. The DGC functions in muscle fiber adhesion by linking the ECM to sarcomeres, and loss of function of this complex leads to muscle wasting and loss of muscle integrity (3). Thus, Sin3A and Sin3B target genes encode components of the sarcomere and adhesion complexes needed to maintain muscle integrity, and aberrant regulation of these genes could represent a molecular basis for the phenotypes observed upon acute somatic inactivation of Sin3A or both Sin3A and Sin3B, including friability of sarcomeres and the apparent disorganization of myofibrils.

Sin3 complexes function as activators on sarcomere genes. Next, we addressed whether Sin3 complexes act as a repressor or activator complex on this set of genes involved in muscle differentiation and physiology. Therefore, we first analyzed the connection between Sin3 binding and expression of these genes in myoblasts and myotubes. Transcript levels corresponding to this subset of genes increased during differentiation for most genes (Fig. 6A). We have previously shown that recruitment of Sin3 complexes to a set of genes repressed in

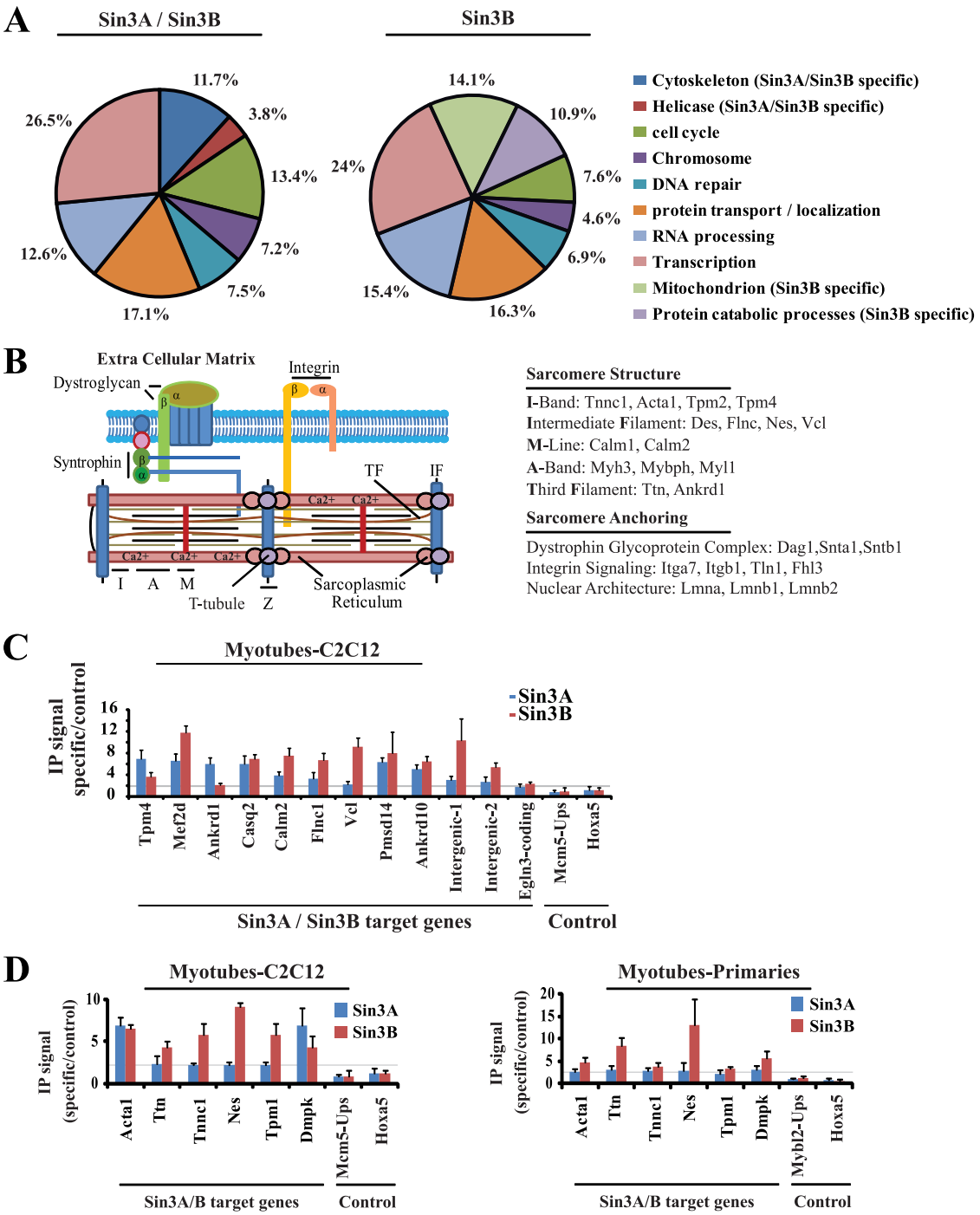

FIG. 5. Annotation and verification of Sin3 target genes. (A) Distribution of GO annotations for Sin3A and Sin3B target genes. Sin3A and Sin3B binding sites within a distance comprising bp −3000 to +3000 relative to the TSS were included in the annotation analysis. In some instances, a gene is assigned to more than one category. The chart depicts the distribution of GO categories among genes bound specifically by Sin3B or both proteins in differentiated myotubes. There were no enriched GO categories for genes bound by Sin3A only. The percentage refers to the number of bound genes within a particular category in relation to the total number of bound genes that have a GO annotation. (B) Sin3A and Sin3B bind to a subset of sarcomeric genes in differentiated myotubes. (Left panel) Schematic showing sarcomere and extracellular matrix (ECM). (Right panel) Sin3 target genes encode components of sarcomeric and ECM compartments. (C) Analysis of Sin3A and Sin3B binding in differentiated C2C12 myotubes by qChIP. The IP signal was defined as the ratio of IP/input for a specific amplicon versus a control amplicon (*Gapdh*). The averages of results from three independent experiments are shown. Error bars represent standard deviations. (D) Analysis of Sin3A and Sin3B binding in differentiated C2C12 myotubes and primary myotubes by ChIP and quantitative real-time PCR. IP signal was defined as the ratio of IP/input for a specific amplicon versus a control amplicon (*Gapdh*). The averages of results from three independent experiments are shown. Error bars represent standard deviations.

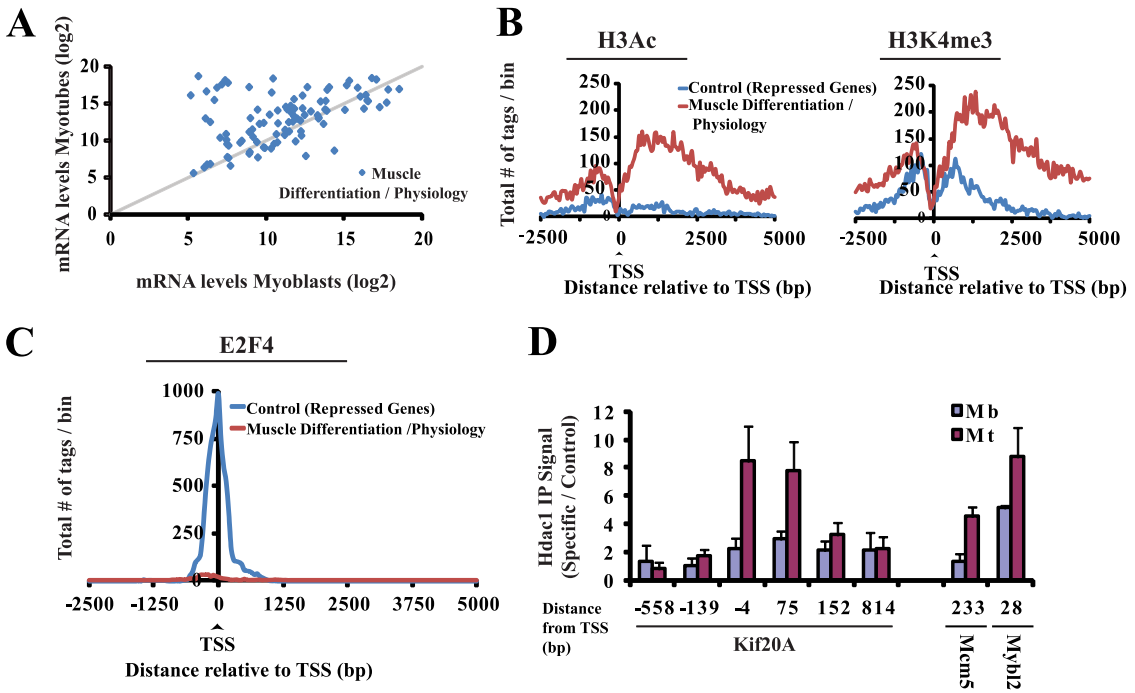

FIG. 6. Sin3A and Sin3B proteins bind to active chromatin on a set of muscle-related genes. (A) Expression of a set of genes involved in muscle differentiation and physiology was analyzed. Values were derived from expression analyses and presented in $\log_2$ scale. (B) Distribution of H3Ac and H3K4me3 marks on genes involved in muscle differentiation and physiology (98 genes) and a group of Sin3 target genes that were repressed in myotubes (85 genes). For both groups, the number of tags per 50-bp bin was counted and plotted relative to the transcription start site. (C) Distribution of E2F4 binding events for genes as described for panel D. (D) Analysis of binding of HDAC1 to selected repressed Sin3 target genes in myoblasts (Mb) and differentiated myotubes (Mt) by ChIP and quantitative real-time PCR. The IP signal was defined as the ratio of IP/input for a specific amplicon versus a control amplicon (*Gapdh*). The averages of results from three independent experiments are shown. Error bars represent standard deviations.

myotubes correlated with the recruitment of E2F4, as well as decreased levels of H3 acetylation (H3Ac) and H3K4 trimethylation (H3K4me3), marks signifying active chromatin (39). Therefore, to further discriminate between repressor and activator complexes, we tested whether Sin3 binding coincided with recruitment of E2F4, H3Ac, and H3K4me3 within the downstream regions of genes involved in muscle and sarcomere structure and function using ChIP-seq. We observed high levels of H3Ac and H3K4me3 and background levels for E2F4 binding on this set of genes, whereas we observed low levels of H3Ac and H3K4me3 and enhanced levels of E2F4 and HDAC1 binding on a set of Sin3 target genes that were repressed (Fig. 6B to D).

In order to determine whether Sin3A and Sin3B directly contribute to activation of a subset of these genes, we analyzed mRNA levels of *ttn*, *ttnc1*, *acta1*, and *dmpk*, which encode proteins critical to the integrity of sarcomeres, in C2C12 and primary myotubes after acute deletion of Sin3A, Sin3B, or both. First, differentiated myotubes were transfected with control or specific siRNAs targeting Sin3A and Sin3B, and differences in mRNA abundance were analyzed using quantitative RT-PCR. We found that expression of most genes bound by both Sin3A and Sin3B was markedly decreased upon depletion of Sin3A and Sin3B (Fig. 7A). In contrast, expression levels of *Brca1* and *Mcm5*, previously shown to be repressed by Sin3-containing E2F4 complexes (39), were increased upon ablation of Sin3A and Sin3B. To further dissect the individual roles of Sin3A and Sin3B, we depleted Sin3A, Sin3B, or both proteins in primary myotubes. Ablation of Sin3B did not result in significant changes in the expression of any of these genes (Fig. 7B). In contrast, we observed significant ($P < 0.05$) reductions in expression of *tnnc1* and *dmpk* after ablation of Sin3A and significant decreases in *ttn*, *acta1*, *tnnc1*, and *dmpk* levels after ablation of both Sin3A and Sin3B. Levels of *Casq2* (a Sin3A and Sin3B target encoding a sarcoplasmic reticulum protein) or *Kif20A* (a target repressed by Sin3-E2F4 [39]) either were not significantly affected or were upregulated, respectively, by inactivation of Sin3A or both Sin3A and Sin3B. Thus, Sin3 complexes act directly and specifically as activators on a subset of these genes in C2C12 and primary myotubes.

We have shown previously that both Sin3 isoforms bind to a large cluster of E2F4 target genes in differentiated myotubes and that ablation of both Sin3 proteins leads to reexpression of a subset of these genes (Fig. 7A and B) (39). In addition, acute ablation of retinoblastoma tumor suppressor protein (pRB) in differentiated myotubes also led to reexpression of an overlapping set of E2F4 and Sin3 target genes, particularly those involved in cell cycle control (5). Therefore, it was important to test whether ablation of Sin3 in differentiated myotubes leads to cell cycle defects, as reported for cycling cells (12, 13). First, we asked whether Sin3 proteins associate with pRB in nuclear extracts derived from myoblasts and myotubes. We found that Sin3A and Sin3B coprecipitated with pRB under both conditions, although we observed significantly weaker interactions in

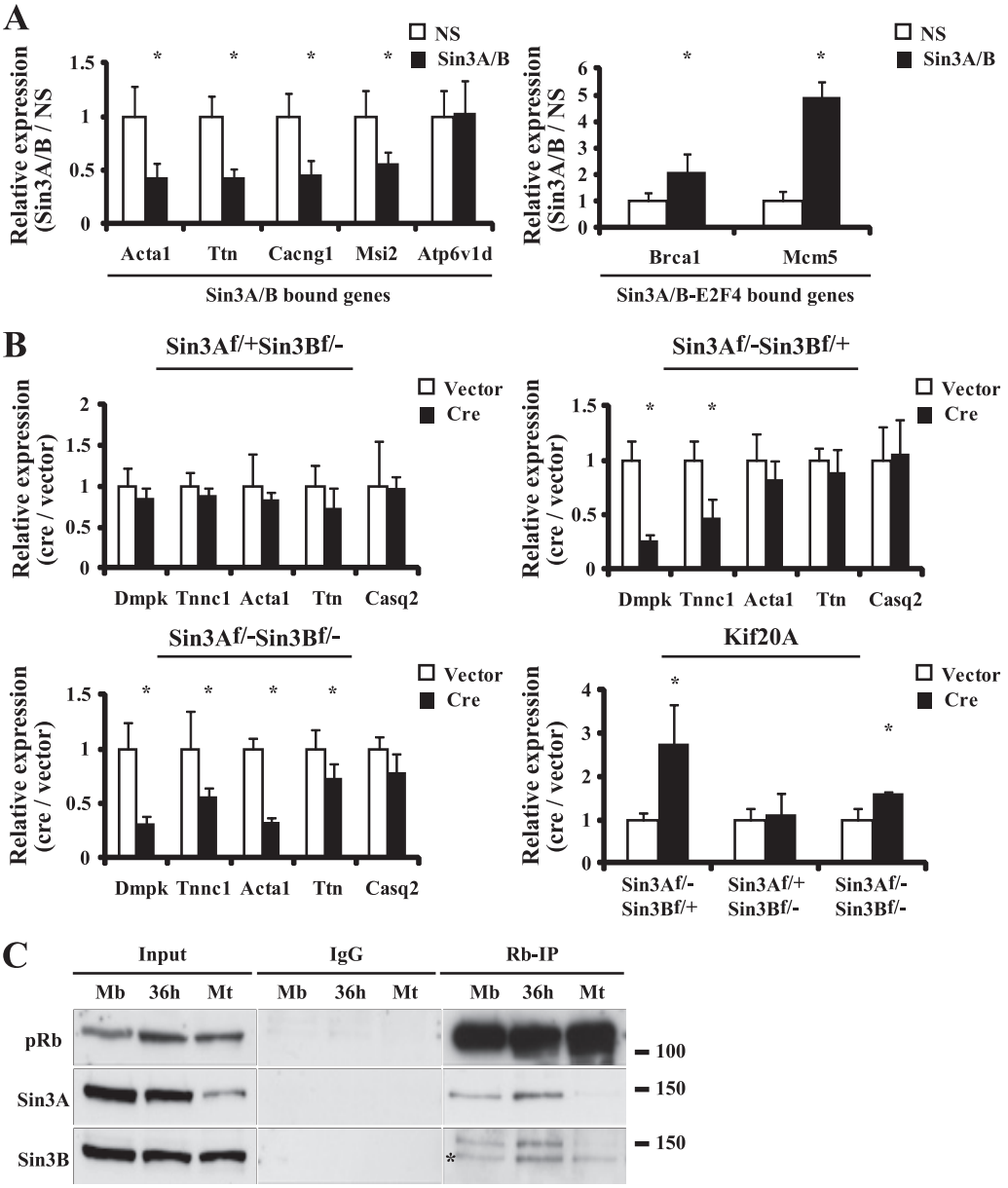

FIG. 7. Sin3A and Sin3B proteins directly control transcription of muscle and sarcomere genes. (A) Gene expression analysis using quantitative real time RT-PCR of selected genes after ablation of both Sin3A and Sin3B in C2C12 myotubes. Myotubes were transfected 48 h after induction of differentiation and were isolated 96 h after transfection. Expression levels of selected genes in Sin3 siRNA-transfected cells were compared to the level for nonspecific control (NS) transfected cells. The averages of results from three independent experiments are shown. Error bars represent standard deviations. (B) Gene expression analysis using quantitative real time RT-PCR of selected genes after ablation of Sin3A, Sin3B, or both proteins. Primary myoblasts were induced to differentiate, and primary myotubes were infected 48 h after induction of differentiation with adenovirus that lacks (Vector) or expresses (Cre) Cre recombinase. The expression levels of control- and Cre-infected cells were normalized to the levels for Rbp2, which is expressed at high levels and not bound by Sin3 in differentiated myotubes. Normalized Cre values were compared with normalized control values. The averages of results from three independent experiments are shown. Error bars represent standard deviations. The asterisk indicates expression levels significantly different from those for the vector control cells ($P < 0.05$ by Student's t test). (C) Endogenous Sin3A and Sin3B interact with pRB during myogenesis. pRB was immunoprecipitated using nuclear extracts of C2C12 myoblasts and differentiated myotubes. All samples were loaded on a single gel, and Western blots were probed for either Sin3A or Sin3B. The asterisk indicates Sin3B protein.

differentiated myotubes (Fig. 7C). Furthermore, we did not observe cell cycle reentry of differentiated myotubes after ablation of both Sin3A and Sin3B or loss of cell viability (data not shown), as reported previously for cycling cells ablated for Sin3A (12). Thus, our observations point to a role for Sin3 proteins in assembling sarcomeres and/or maintaining sarcomere integrity, and this phenotype is independent of defects in cell cycle control or apoptosis.

Compensatory changes associated with loss of Sin3A. Surprisingly, our phenotypic and expression analyses of muscle cells after conditional ablation of Sin3 proteins did not point to a specific role for Sin3B in maintenance of muscle integrity, in

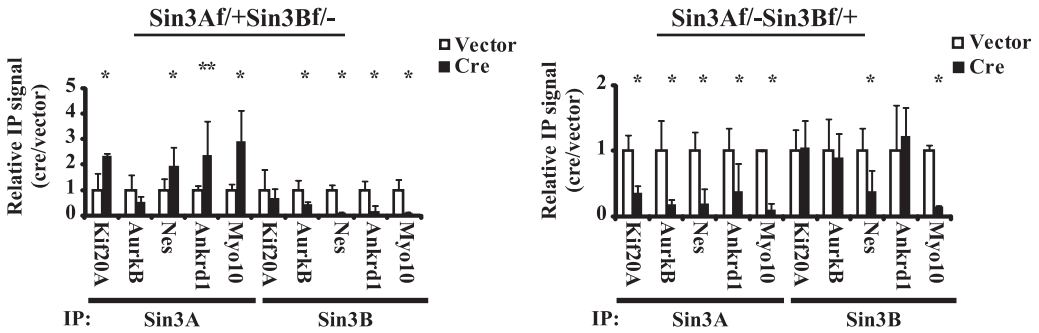

FIG. 8. Increased Sin3A binding compensates for the loss of Sin3B binding on selected genes. qChIP analysis of Sin3A and Sin3B binding in differentiated primary myotubes ablated for Sin3A or Sin3B was done as described for Fig. 4B. Relative binding is represented by the ratio of signals obtained in Cre- and vector-infected primary myotubes. Error bars represent standard deviations. The asterisk indicates a Sin3A or Sin3B binding signal significantly different from that for the vector control cells ($P < 0.05$ by Student's t test). The double asterisk indicates a P value of <0.07 by Student's t test for Ankrd1 only.

contrast with what was found for Sin3A, although we observed strong binding of Sin3B to genes related to this function. We speculated that Sin3A could compensate for the loss of Sin3B on this set of genes and that the combined loss of both proteins is required to fully reveal defects in gene transcription and subsequent phenotypic changes. To test this notion, we performed ChIP assays for Sin3A and Sin3B after ablation of either gene in differentiated primary myotubes. As expected, recruitment of both proteins diminished significantly after ablation, according to their respective genotypes (Fig. 8). Remarkably, deletion of Sin3B led to an upregulation of Sin3A binding on selected genes (*Kif20A*, *Nes*, *Ankrd1*, and *Myo10*) (Fig. 8, left panel). However, we did not observe increased binding of Sin3B after ablation of Sin3A. Instead, we observed dramatic decreases in Sin3B binding on two genes, *Nes* and *Myo10*, after removal of Sin3A (Fig. 8, right panel). We have shown that Sin3A associates with Sin3B in myotubes, consistent with the notion that both isoforms may be coordinately recruited to certain genes (39). Collectively, our data (i) strongly suggest that a subset of sarcomeric genes are directly activated by Sin3A and Sin3B and (ii) provide a molecular explanation for the enhanced phenotype observed upon inactivation of both Sin3A and Sin3B, compared to what was found for inactivation of Sin3A alone, and the lack of overt alterations associated with inactivation of Sin3B *in vivo* and *in vitro* (Fig. 2 and 3).

In summary, our results reveal distinct roles for Sin3A and Sin3B proteins in maintaining myofibril function in the post-differentiated state and provide insights into a positive role for Sin3 isoforms in context-specific gene expression. Sin3 complexes could be recruited by muscle-specific transcription factors to promote expression of target genes identified herein. More broadly, it was shown that binding of mammalian HDAC1 complexes promotes histone deacetylation within the coding regions of active genes (40). Restoring the balance of acetylation levels in the wake of polymerase II (Pol II) transcription could provide a mechanism for maintaining a chromatin environment permissive for multiple rounds of Pol II elongation and for preventing antisense and cryptic expression (22, 24). This could be particularly relevant for sarcomere genes, which are transcribed at high rates in differentiated myotubes. Therefore, it will be important to determine whether mammalian Sin3-containing complexes identified here associate with histone deacetylases and whether these complexes are involved in suppressing aberrant transcription. This will be especially interesting in light of results for yeast, wherein a Sin3 complex was shown to bind within coding regions of active genes to suppress spurious transcription (8, 18, 27). Interestingly, the histone H3 lysine 4 demethylase Kdm5a protein (also known as Rbp2 and Jarid1a) could play a role in transcriptional activation of Sin3 target genes. We have previously shown that Kdm5a associates with Sin3 proteins in differentiated myotubes (39). In *Drosophila* species, the Kdm5a homolog Lid was shown to function as an activator (23, 34). Lid physically interacts with Rpd3 and inhibits its deacetylase activity *in vitro* and *in vivo* (23). It is important to note that, besides HDACs and Kdm5a, Sin3 complexes associate with other regulatory proteins, including Swi/Snf and ING1/2 (36). Thus, in order to elucidate the molecular mechanism of Sin3-mediated gene transcription, it will be important to fully characterize the composition of Sin3 complexes in differentiated myotubes and to further discriminate between repressor and activator Sin3 complexes.

ACKNOWLEDGMENTS

We are especially thankful to A. Liang and E. Roth for invaluable assistance with all EM studies conducted at the Skirball Imaging Facility. We are grateful to colleagues in the Dynlacht laboratory for advice and to S. Brown and Z. Tang for assistance with analysis of Illumina/Solexa 2G sequencing.

This work was supported by funds from the NIH (2R01GM067132-05A1 and 2R01CA077245-12A1) to B.D.D. and from ACS (RSG-08-054-01-GMC) to G.D.

REFERENCES

1. **Alland, L., R. Muhle, H. Hou, Jr., J. Potes, L. Chin, N. Schreiber-Agus, and R. A. DePinho.** 1997. Role for N-CoR and histone deacetylase in Sin3-mediated transcriptional repression. Nature **387:**49–55.
2. **Ayer, D. E., Q. A. Lawrence, and R. N. Eisenman.** 1995. Mad-Max transcriptional repression is mediated by ternary complex formation with mammalian homologs of yeast repressor Sin3. Cell **80:**767–776.
3. **Batchelor, C. L., and S. J. Winder.** 2006. Sparks, signals and shock absorbers: how dystrophin loss causes muscular dystrophy. Trends Cell Biol. **16:**198–205.
4. **Blais, A., M. Tsikitis, D. Acosta-Alvear, R. Sharan, Y. Kluger, and B. D. Dynlacht.** 2005. An initial blueprint for myogenic differentiation. Genes Dev. **19:**553–569.
5. **Blais, A., C. J. van Oevelen, R. Margueron, D. Acosta-Alvear, and B. D. Dynlacht.** 2007. Retinoblastoma tumor suppressor protein-dependent meth-

ylation of histone H3 lysine 27 is associated with irreversible cell cycle exit. J. Cell Biol. **179:**1399–1412.
6. **Bruning, J. C., M. D. Michael, J. N. Winnay, T. Hayashi, D. Horsch, D. Accili, L. J. Goodyear, and C. R. Kahn.** 1998. A muscle-specific insulin receptor knockout exhibits features of the metabolic syndrome of NIDDM without altering glucose tolerance. Mol. Cell **2:**559–569.
7. **Burkin, D. J., and S. J. Kaufman.** 1999. The alpha7beta1 integrin in muscle development and disease. Cell Tissue Res. **296:**183–190.
8. **Carrozza, M. J., B. Li, L. Florens, T. Suganuma, S. K. Swanson, K. K. Lee, W. J. Shia, S. Anderson, J. Yates, M. P. Washburn, and J. L. Workman.** 2005. Histone H3 methylation by Set2 directs deacetylation of coding regions by Rpd3S to suppress spurious intragenic transcription. Cell **123:**581–592.
9. **Cavellan, E., P. Asp, P. Percipalle, and A. K. Farrants.** 2006. The WSTF-SNF2h chromatin remodeling complex interacts with several nuclear proteins in transcription. J. Biol. Chem. **281:**16264–16271.
10. **Cowley, S. M., B. M. Iritani, S. M. Mendrysa, T. Xu, P. F. Cheng, J. Yada, H. D. Liggitt, and R. N. Eisenman.** 2005. The mSin3A chromatin-modifying complex is essential for embryogenesis and T-cell development. Mol. Cell. Biol. **25:**6990–7004.
11. **Cunliffe, V. T.** 2008. Eloquent silence: developmental functions of Class I histone deacetylases. Curr. Opin. Genet. Dev. **18:**404–410.
12. **Dannenberg, J. H., G. David, S. Zhong, J. van der Torre, W. H. Wong, and R. A. Depinho.** 2005. mSin3A corepressor regulates diverse transcriptional networks governing normal and neoplastic growth and survival. Genes Dev. **19:**1581–1595.
13. **David, G., K. B. Grandinetti, P. M. Finnerty, N. Simpson, G. C. Chu, and R. A. Depinho.** 2008. Specific requirement of the chromatin modifier mSin3B in cell cycle exit and cellular differentiation. Proc. Natl. Acad. Sci. U. S. A. **105:**4168–4172.
14. **Dennis, G., Jr., B. T. Sherman, D. A. Hosack, J. Yang, W. Gao, H. C. Lane, and R. A. Lempicki.** 2003. DAVID: Database for Annotation, Visualization, and Integrated Discovery. Genome Biol. **4:**P3.
15. **Heinzel, T., R. M. Lavinsky, T. M. Mullen, M. Soderstrom, C. D. Laherty, J. Torchia, W. M. Yang, G. Brard, S. D. Ngo, J. R. Davie, E. Seto, R. N. Eisenman, D. W. Rose, C. K. Glass, and M. G. Rosenfeld.** 1997. A complex containing N-CoR, mSin3 and histone deacetylase mediates transcriptional repression. Nature **387:**43–48.
16. **Huh, M. S., M. H. Parker, A. Scime, R. Parks, and M. A. Rudnicki.** 2004. Rb is required for progression through myogenic differentiation but not maintenance of terminal differentiation. J. Cell Biol. **166:**865–876.
17. **Kadosh, D., and K. Struhl.** 1997. Repression by Ume6 involves recruitment of a complex containing Sin3 corepressor and Rpd3 histone deacetylase to target promoters. Cell **89:**365–371.
18. **Keogh, M. C., S. K. Kurdistani, S. A. Morris, S. H. Ahn, V. Podolny, S. R. Collins, M. Schuldiner, K. Chin, T. Punna, N. J. Thompson, C. Boone, A. Emili, J. S. Weissman, T. R. Hughes, B. D. Strahl, M. Grunstein, J. F. Greenblatt, S. Buratowski, and N. J. Krogan.** 2005. Cotranscriptional set2 methylation of histone H3 lysine 36 recruits a repressive Rpd3 complex. Cell **123:**593–605.
19. **Kurdistani, S. K., D. Robyr, S. Tavazoie, and M. Grunstein.** 2002. Genome-wide binding map of the histone deacetylase Rpd3 in yeast. Nat. Genet. **31:**248–254.
20. **Laherty, C. D., W. M. Yang, J. M. Sun, J. R. Davie, E. Seto, and R. N. Eisenman.** 1997. Histone deacetylases associated with the mSin3 corepressor mediate mad transcriptional repression. Cell **89:**349–356.
21. **Laing, N. G., and K. J. Nowak.** 2005. When contractile proteins go bad: the sarcomere and skeletal muscle disease. Bioessays **27:**809–822.
22. **Lee, J. S., and A. Shilatifard.** 2007. A site to remember: H3K36 methylation a mark for histone deacetylation. Mutat. Res. **618:**130–134.
23. **Lee, N., H. Erdjument-Bromage, P. Tempst, R. S. Jones, and Y. Zhang.** 2009. The H3K4 demethylase lid associates with and inhibits histone deacetylase Rpd3. Mol. Cell. Biol. **29:**1401–1410.
24. **Li, B., M. Carey, and J. L. Workman.** 2007. The role of chromatin during transcription. Cell **128:**707–719.
25. **McDonel, P., I. Costello, and B. Hendrich.** 2009. Keeping things quiet: roles of NuRD and Sin3 co-repressor complexes during mammalian development. Int. J. Biochem. Cell Biol. **41:**108–116.
26. **McNally, E. M., and P. Pytel.** 2007. Muscle diseases: the muscular dystrophies. Annu. Rev. Pathol. **2:**87–109.
27. **Nicolas, E., T. Yamada, H. P. Cam, P. C. Fitzgerald, R. Kobayashi, and S. I. Grewal.** 2007. Distinct roles of HDAC complexes in promoter silencing, antisense suppression and DNA damage protection. Nat. Struct. Mol. Biol. **14:**372–380.
28. **Pile, L. A., P. T. Spellman, R. J. Katzenberger, and D. A. Wassarman.** 2003. The SIN3 deacetylase complex represses genes encoding mitochondrial proteins: implications for the regulation of energy metabolism. J. Biol. Chem. **278:**37840–37848.
29. **Rando, T. A., and H. M. Blau.** 1994. Primary mouse myoblast purification, characterization, and transplantation for cell-mediated gene therapy. J. Cell Biol. **125:**1275–1287.
30. **Rayman, J. B., Y. Takahashi, V. B. Indjeian, J. H. Dannenberg, S. Catchpole, R. J. Watson, H. te Riele, and B. D. Dynlacht.** 2002. E2F mediates cell cycle-dependent transcriptional repression in vivo by recruitment of an HDAC1/mSin3B corepressor complex. Genes Dev. **16:**933–947.
31. **Robert, F., D. K. Pokholok, N. M. Hannett, N. J. Rinaldi, M. Chandy, A. Rolfe, J. L. Workman, D. K. Gifford, and R. A. Young.** 2004. Global position and recruitment of HATs and HDACs in the yeast genome. Mol. Cell **16:**199–209.
32. **Schreiber-Agus, N., L. Chin, K. Chen, R. Torres, G. Rao, P. Guida, A. I. Skoultchi, and R. A. DePinho.** 1995. An amino-terminal domain of Mxi1 mediates anti-Myc oncogenic activity and interacts with a homolog of the yeast transcriptional repressor SIN3. Cell **80:**777–786.
33. **Schwander, M., M. Leu, M. Stumm, O. M. Dorchies, U. T. Ruegg, J. Schittny, and U. Muller.** 2003. Beta1 integrins regulate myoblast fusion and sarcomere assembly. Dev. Cell **4:**673–685.
34. **Secombe, J., L. Li, L. Carlos, and R. N. Eisenman.** 2007. The Trithorax group protein Lid is a trimethyl histone H3K4 demethylase required for dMyc-induced cell growth. Genes Dev. **21:**537–551.
35. **Sharma, V., A. Swaminathan, R. Bao, and L. A. Pile.** 2008. Drosophila SIN3 is required at multiple stages of development. Dev. Dyn. **237:**3040–3050.
36. **Silverstein, R. A., and K. Ekwall.** 2005. Sin3: a flexible regulator of global gene expression and genome stability. Curr. Genet. **47:**1–17.
37. **Takahashi, Y., J. B. Rayman, and B. D. Dynlacht.** 2000. Analysis of promoter binding by the E2F and pRB families in vivo: distinct E2F proteins mediate activation and repression. Genes Dev. **14:**804–816.
38. **Tallquist, M. D., K. E. Weismann, M. Hellstrom, and P. Soriano.** 2000. Early myotome specification regulates PDGFA expression and axial skeleton development. Development **127:**5059–5070.
39. **van Oevelen, C., J. Wang, P. Asp, Q. Yan, W. G. Kaelin, Jr., Y. Kluger, and B. D. Dynlacht.** 2008. A role for mammalian Sin3 in permanent gene silencing. Mol. Cell **32:**359–370.
40. **Wang, Z., C. Zang, K. Cui, D. E. Schones, A. Barski, W. Peng, and K. Zhao.** 2009. Genome-wide mapping of HATs and HDACs reveals distinct functions in active and inactive genes. Cell **138:**1019–1031.
41. **Zhang, Y., T. Liu, C. A. Meyer, J. Eeckhoute, D. S. Johnson, B. E. Bernstein, C. Nussbaum, R. M. Myers, M. Brown, W. Li, and X. S. Liu.** 2008. Model-based analysis of ChIP-Seq (MACS). Genome Biol. **9:**R137.